CHAPTER II

THEORITICAL BACKGROUND

2.1 Theory

ATR FT-IR spectroscopy stands for attenuated total reflection Fourier transform infrared spectroscopy. It is a material characterization technique using an internal reflection principle. The total internal reflection is an optical phenomenon, which can be observed easily, for example, with a glass of water. If the side of the glass below the water level is viewed obliquely through the water surface, it appears to be completely silvered and one can no longer see objects behind it. The reason for this is that light striking the glass surface is totally reflected and therefore does not pass through the surface to illuminate these objects.

The unusual characteristics associated with total internal reflection can be utilized in many areas. These applications include precision measurements of angles and refractive indices; the construction of beam splitters, optical filters, laser cavities, light modulators, light deflectors; and the measurement of film thicknesses and surface reliefs.

When light travels in a medium with high refractive index (i.e., a denser medium) impinge at the interface with a medium of lower refractive index (i.e., a rarer medium) at an angle greater than the critical angle, total reflection occurs. The critical angle can be calculated from the refractive indices of the denser medium and the rarer medium by the following expression [17]:

$$\theta_c = \sin^{-1}(n_1/n_0) \tag{2.1}$$

where n_0 and n_1 are the refractive indices of the denser medium and that of the rarer medium, respectively.

Under non-absorbing condition (i.e., the rarer medium is transparent or absorption index of the medium equals zero), the incident light is totally reflected at the interface. Since there is no light travel across the interface, no reflection loss due to absorption is observed. This phenomenon is defined as total reflection phenomenon. When the rarer medium is absorbing (i.e., its absorption index is greater than zero), there is a reflection loss due to absorption. Reflectance of the beam leaving IRE/sample interface is less than unity. This phenomenon is defined as attenuated total reflection (ATR) phenomenon.

In an ATR configuration, the denser medium (i.e., an internal reflection element, IRE) is in contact with an optically rarer medium (i.e., a sample) as shown in Figure 2.1. The IRE is infrared transparent and has a refractive index n_0. The sample is infrared absorbing and has a complex refractive index at frequency v (cm^{-1}) of [17]:

$$\hat{n}_1 = n_1 + ik_1 \tag{2.2}$$

where i is equal to $\sqrt{-1}$, n_1 and k_1 are refractive index and absorption index, respectively. The absorption index is directly related to the absorption coefficient, α, by the following expression [17]:

$$\alpha(v) = 4\pi v k(v) \tag{2.3}$$
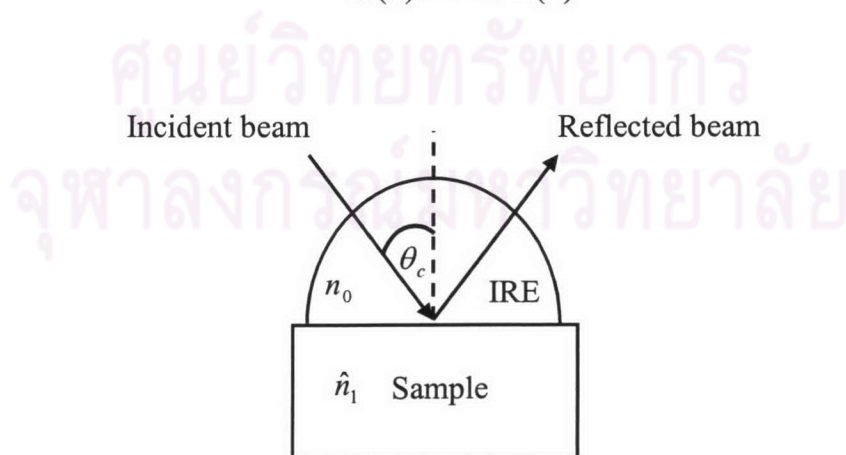
Figure 2.1 Ray tracing under total internal reflection.

Under the ATR condition, although there is no light travels across the IRE/sample interface. There exists a strong electric field at the interface. The field is known as the evanescent field. The field is strongest at the interface. It exponentially decays to zero within a few micrometers from surface of the IRE. The field interacts with the sample and causes a reflection loss in the reflected beam.

The rapid decay of the evanescent field is the unique characteristic that makes ATR technique a surface characterization technique. The decay characteristic of the evanescent field can be expressed in terms of the distance from the IRE/sample interface by the following expression [1]:

$$E_z = E_0 e^{-2z/d_p} \tag{2.4}$$

where E_0 and E_z are the evanescent fields at the IRE/sample interface and at depth z in the sample, respectively while d_p is the penetration depth. The penetration depth is defined by the distance from the interface where the evanescent field decays to $1/e$ of its strength at the interface. The penetration depth is given in terms of experimental condition and material characteristics by [1]:

$$d_p = \frac{1}{2\pi v n_0 (\sin^2 \theta - (n_1/n_0)^2)^{1/2}} \tag{2.5}$$

where $v(cm^{-1})$ is the frequency of the IR radiation and θ is the angle of incidence. The evanescent field characteristic at the boundary between IRE and sample is shown in Figure 2.2.[1]
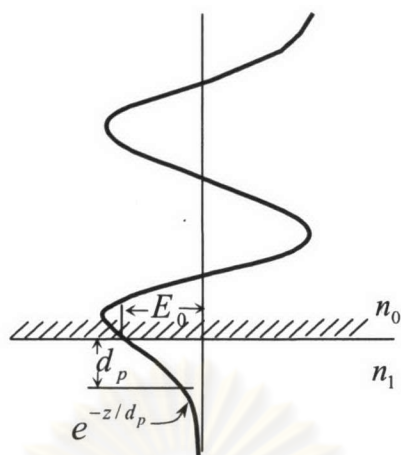
Figure 2.2 Evanescent wave at the boundary between IRE and sample.

According to equation 2.5, there are several important parameters that affect the observed spectrum and spectral qualities. One of them is the index matching. At a fixed angle of incidence, the penetration depth is larger for better index matching (i.e., n_1 is similar to n_0). The refractive indices of standard IRE span from 2.4 to 4.0. When an organic material (refractive index of 1.5) is placed in contact with a ZnSe IRE (refractive index of 2.4), the ratio of the refractive indices is $(n_1/n_0) = 0.625$. In contrary, when an organic material is in contact with a germanium IRE (refractive index of 4.0), the ratio of the refractive indices becomes 0.375. According to equation 2.5, the penetration depth with ZnSe as the IRE is greater than that with Ge. The expression also indicates that the penetration depth depend largely on the frequency of the incident beam. As the frequency of the infrared light increases the penetration depth decreases. However in practice, it is often convenient to express frequency in terms of wavenumber, the penetration depth decreases when wavenumber increases. This also leads to a decrease of relative band intensities in the ATR spectrum with increasing wavenumber when compared to the corresponding transmission spectrum. Furthermore, changing the angle of incident changes the penetration depth. If the angle of incident is increased, the penetration depth will be decreased and the spectral intensity will be decreased. The greater penetration depth implies a greater distance from surface of the sample where chemical information can be observed by ATR technique.

2.2 Internal Reflection Elements

The internal reflection element (IRE) is an infrared transparent material used in internal reflection spectroscopy for establishing the conditions necessary to obtain internal reflection spectra of materials (see Figure 2.3). Radiation is propagated through the IRE by means of total internal reflection. The sample material is placed to contact with the surface of IRE. The ease of obtaining an internal reflection spectrum and the information obtained from the spectrum are determined by a number of characteristics of the IRE. A choice must be made in the working angle or range of angles of incidence, number of reflections, aperture, number of passes, surface preparation, and material from which it is made. [1]

Figure 2.3 Selected IRE configurations commonly used in ATR experiment: (a) single reflection variable-angle hemispherical or hemicylinder crystal, and (b) multiple reflection single-pass crystal.

Table 2.1 Optical constants and transmission regions of IRE materials. [18]

Material	Useful range, cm^{-1}	Reflective index At 1000 cm^{-1}
Zinc selenide, ZnSe	20,000-460	2.42
Thallium iodide/bromide ,KRS-5	20,000-250	2.37
Gemanium, Ge	5,500-600	4.0
Silicon, Si	8,300-660	3.4
Diamond, C	45,000-~2,500, ~1650-200	2.417

The choice of an internal reflection element is very important. Table 2.1 lists the characteristics of the most common internal reflection elements. KRS-5 is the trade name for thallium iodide/thallium bromide. This material is extremely toxic, and should only be handled with care by wearing gloves. It is a useful material because its transmission range covers the entire mid-infrared. The disadvantage of KRS-5 is that it is a soft material and can be easily scratched or bent. Zinc selenide, ZnSe, is the most commonly used ATR crystal. It has good optical performance, it is essentially water insoluble, and it is transparent down to approximately 460 cm^{-1}. Although it is a moderately hard material (hardness = 5) [19], it does scratch and will wear over time. It is also chemically reactive: the surface is ionic in nature, acidic and alkaline media attack the surface. Silicon (Si) and germanium (Ge) are also very hard (Hardness of Ge = 6) [20], and are not affected even by strong acids. They are usually employed when very small penetration depths are desired. Diamond is particularly a good internal reflection element since it is the hardest substance known (Hardness = 10) [21], it is

chemically inert, and it is optically transparent. Consequently, hard, abrasive, or corrosive samples are readily analyzed without harming the sample interface, and cleaning the IRE between samples is greatly simplified. All of these features make diamond ATR an ideal choice for hazardous materials analysis, where unknown substance must be identified accurately.

2.3 Spectral Intensity

In ATR experiment, the magnitudes of the interaction between light and the sample can be expressed in terms of absorbance. The absorbance depends on both the material properties (e.g., refractive index of the IRE and complex refractive index of the sample) and the experimental parameters (e.g., angle of incidence and polarization of the incident beam). The relationship between absorbed and reflected intensity in an ATR spectrum is given by [22]:

$$A_l(\theta, v) = 1 - R_l(\theta, v) \tag{2.6}$$

where $A(\theta, v)$ and $R(\theta, v)$ are absorptance and reflectance, respectively and indicates the polarization of the incident beam. The polarization direction is given with respect to the plane of incidence. The plane of incidence is defined as the plane that contains both incident and reflected beam. For p-polarization, the electric component of the electromagnetic wave is parallel to the plane of incidence while the magnetic component is perpendicular to the plane of incidence. Whereas, the electric component of the electromagnetic wave with s-polarization is perpendicular to the plane of incidence while the magnetic component is parallel to the plane of incidence. In general, absorptance in ATR can be expressed in terms of experimental parameters and material characteristic by the following expression [22]:

$$A_l(\theta, v) = \frac{4\pi v}{n_0 \cos\theta} \int_0^\infty n_1(v) k_1(v) \left\langle E_{zl}^2(\theta, v) \right\rangle dz \tag{2.7}$$

where $\langle E_{zl}^2(\theta, v) \rangle$ is the mean square electric field (MSEF) at depth z.

Under a small absorption condition, the decay behavior of the MSEF is the same as that of the mean square evanescent field (MSEvF). Therefore, the MSEF can be estimated from the MSEvF by [22]:

$$\langle E_{zl}^2(\theta, v) \rangle = \frac{1 + R_l(\theta, v)}{2} \langle E_{zl}^2(\theta, v) \rangle_{k=0}$$

$$\langle E_{zl}^2(\theta, v) \rangle = \frac{1 + R_l(\theta, v)}{2} \langle E_{0l}^2(\theta, v) \rangle_{k=0} e^{-2z/d_p} \tag{2.8}$$

where $\langle E_{0l}^2(\theta, v) \rangle_{k=0}$ and $\langle E_{zl}^2(\theta, v) \rangle_{k=0}$ are the MSEvF at the interface between the IRE and the sample and at depth z, respectively.

From equations 2.7 and 2.8, absorptance of an isotropic medium is given in term the MSEvF by [22]:

$$A_l(\theta, v) = \frac{4\pi v}{n_0 \cos\theta} \int_0^\infty n_1(v) k_1(v) \frac{1 + R_l(\theta, v)}{2} \langle E_{zl}^2(\theta, v) \rangle_{k=0} dz$$

$$2\frac{1 - R_l(\theta, v)}{1 + R_l(\theta, v)} = \frac{4\pi v}{n_0 \cos\theta} \int_0^\infty n_1(v) k_1(v) \langle E_{zl}^2(\theta, v) \rangle_{k=0} dz$$

$$-\ln R_l(\theta, v) \cong \frac{4\pi v}{n_0 \cos\theta} \int_0^\infty n_1(v) k_1(v) \langle E_{zl}^2(\theta, v) \rangle_{k=0} dz \tag{2.9}$$

In general, the ATR spectral intensity that obtains from a spectrometer is in absorbance unit. The spectral intensity in absorbance unit is defined in terms of the reflectance by [22]:

$$A_l(\theta, v) = -\log[(R_l\theta, v)] \tag{2.10}$$

According to equations 2.9 and 2.10, an ATR spectral intensity in absorbance unit is given in term of experimental conditions and material characteristics by [23]:

$$A_l(\theta,v) \cong \frac{4\pi v}{\ln(10)\,n_0\cos\theta} \int_0^\infty n_1(v)k_1(v)\left\langle E_{zl}^2(\theta,v)\right\rangle_{k=0} dz \qquad (2.11)$$

The above expression indicates that the MSEvF is one of the important factors that affect the ATR spectral intensity. The MSEvF depends on both the angle of incidence and frequency of the incident beam as shown in Figures 2.3 and 2.4, respectively [23].
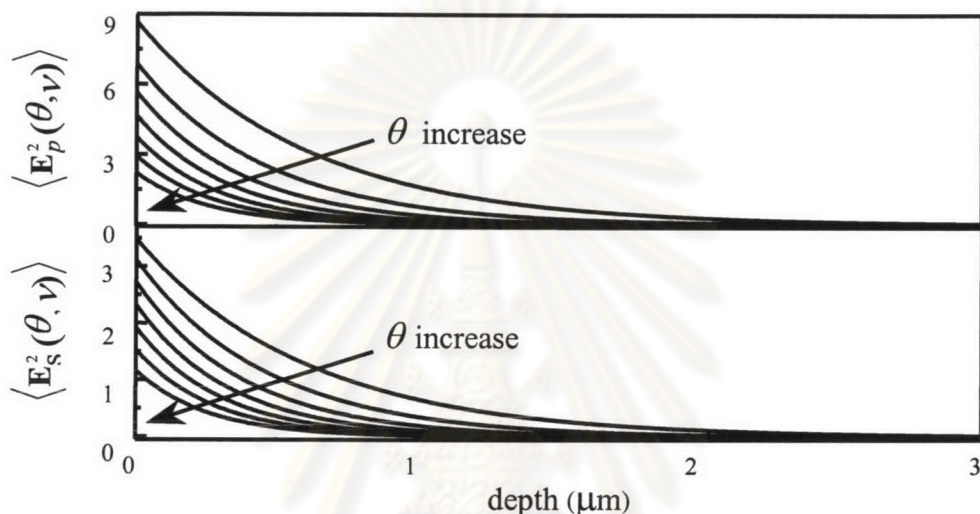
Figure 2.4 Depth dependent MSEvF at various angles of incidences. The simulation parameters are $v = 1000$ cm^{-1}, $n_0 = 4.0$, $n_1 = 1.5$, $k_1 = 0$, $\theta = 30°$, 35°, 40°, 45°, 50°, 55°, 60°
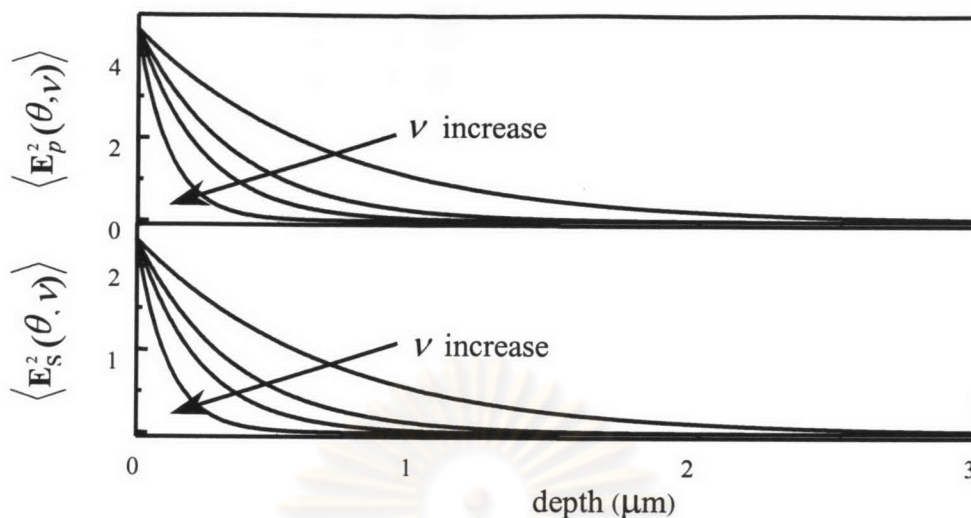
Figure 2.5 Depth dependent MSEvF at various frequencies. The simulation parameter are $n_0 = 4.0$, $n_1 = 1.5$, $k_1 = 0$, $v = 500, 1000, 1500, 3000 \text{ cm}^{-1}$

As the angle of incidence increases, the MSEF at the surface (i.e., z = 0) becomes smaller. The greater the angle of incidence is, the faster the field decays. Figure 2.4 indicates that if the refractive indices at two different frequencies are the same, the MSEF at the surface are the same but their decay characteristics are different. The greater the frequency is, the faster the field decays. Since the evanescent wave decays rapidly with the distance from the surface, it is important to have a good contact between IRE and sample.

2.4 Problem in Optical Contact Between Sample and IRE

As mentioned previously, an optical contact between the IRE and the sample is required in the ATR measurement. Liquid samples always have optical contact with the IRE. Solid sample, on the other hand, rarely have a good contact with IRE. There is always an air gap between the sample and IRE. When there is an air gap in the system, the spectral intensity is severely deteriorated. Since the refractive index of an air gap is 1.0 while that of the organic sample is approximately 1.5, the strength and

decays characteristic of the MSEvF in the system with an air gap is altered by the refractive index mismatch. The unusual decay behavior of the MSEvF with *p*-polarization and *s*-polarization are shown in Figure 2.5. The Figure indicates that the MSEvF with *p*-polarization is altered by the air gap compared to that of the *s*-polarization. Since a part of the strong electric field is occupied by the air gap, which does not involve in any absorption, absorbance of the sample in ATR spectra is decreased. The magnitude of reduction depends largely on the thickness of the air gap. The greater is the air gap, the smaller is the absorbance. In a worse case, spectrum of the sample cannot be observed since the MSEvF decays to zero within the thickness of the air gap. Moreover, the relationship between the absorbance and material characteristics in a system with an air gap does not follow the expression given in Equation 2.11. As a result, the quantitative characteristic of the sample cannot be drawn from such a spectrum.
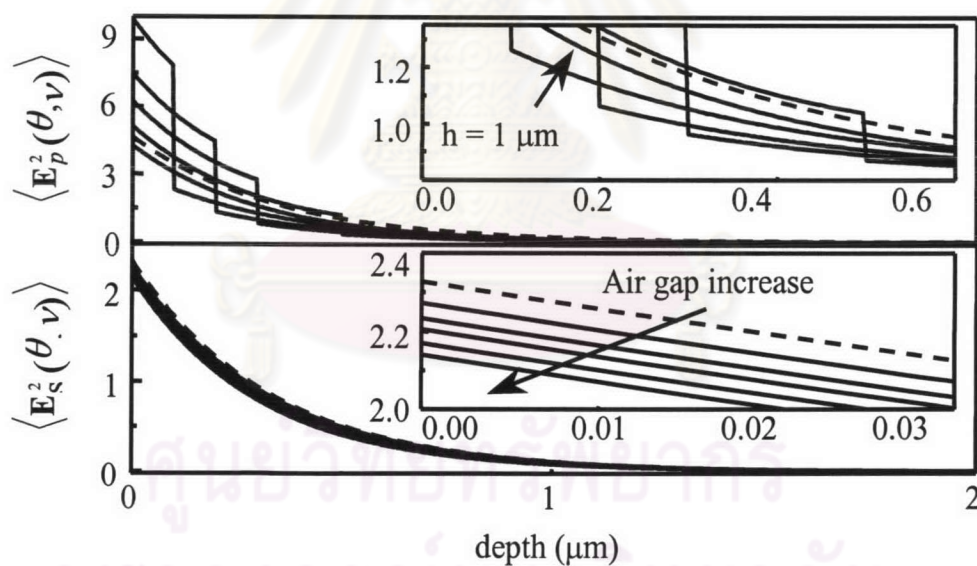
Figure 2.6   The decay characteristic of the MSEvF at various air gap thicknesses (solid lines) and those under optical contact (broken lines). The simulation parameters are $n_0 = 4.0$, $\theta = 45^\circ$, $v = 1000$ cm^{-1}, $n_{air} = 1.0$, $n_F = 1.5$, and the air gap thickness of 0.0, 0.1, 0.2, 0.3, 0.5, and 1.0 μm.

2.5 Diamond is one of the internal reflection elements

### 2.5.1 Model brilliant cut diamond

Diamond has to be cut and shaped to maximize their appeal (see in Figure 2.7). Historically, gem cutting and shaping techniques have been perfected with diamond and the so called brilliant cut with 57+1 facets has become the standard. The faceting and angle of cut is chosen, taking into account the refractive index and dispersion [24] (see Figures 2.7 and 2.8).

Figure 2.7 Popular diamond cuts. The picture shows three different views of the brilliant cut, with 57 facets. **a,** crown with 32 facets, plus the large table facet; **b,** side view; and **c,** pavilion with 16 lower girdle and 8 pavilion facets. If there is a culet facet, the total will be 58 facets.
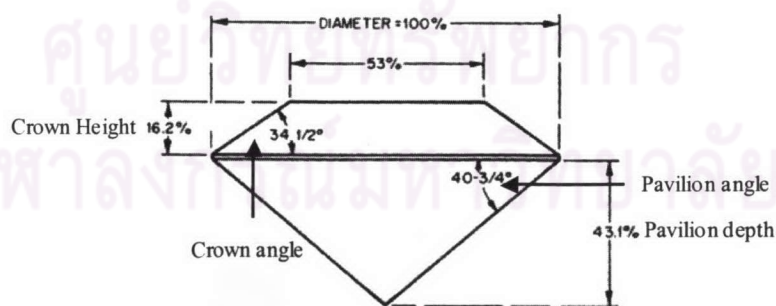

Figure 2.8 An optimum proportion and angles of cut for diamond.
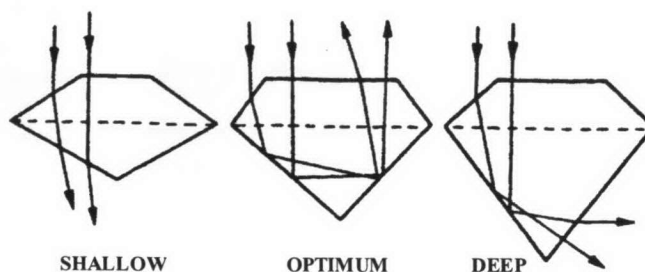
Figure 2.9 A correctly proportioned diamond returns almost all the light entering, by total internal reflections. This will result in maximum brilliance as shown at the center. A shallow cut or deep cut leads to leakage of light and loss of brilliance.

2.5.2 Total internal reflection in a diamond

When light strikes the outside surface of a clean, well-polished diamond, some of that incident light is reflected back from the surface. The remaining incident light is refracted, which means that it is transmitted (or enters) through the surface and into the diamond. The amount of reflection depends on the optical properties of the material. With its high refractive index, diamond is one of the most reflective of all gems (RI = 2.417). For example, 17% of all the light that strikes perpendicular (the angle of incident = 0° which measured from an imaginary line perpendicular to the surface at the point where the light strikes) to a well-polished diamond's outer surface is reflected back, whereas only 4% would be reflected from well-polished glass. This leads to one of diamond's many appealing characteristics: clean, well-polished diamond-facet surfaces display a very high luster when compared to other gem materials.
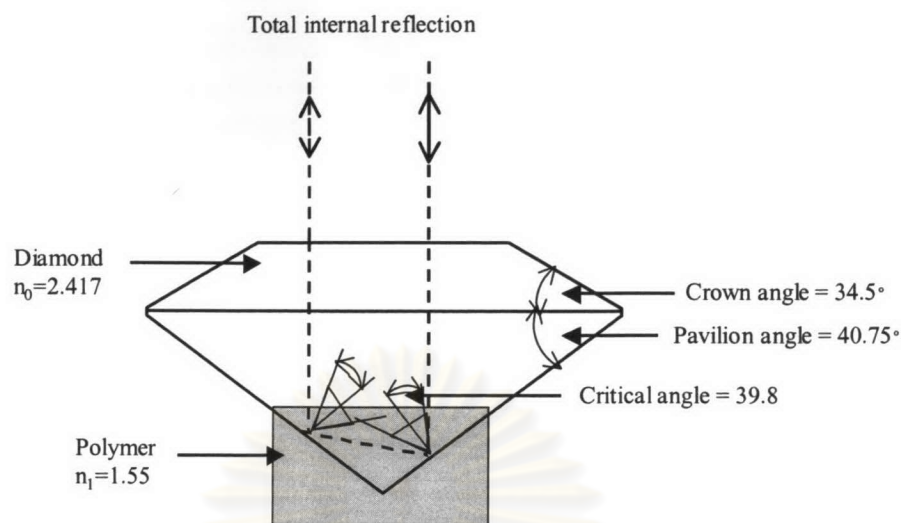
Figure 2.10 Travel paths of the infrared beam and total internal reflection phenomenon in the faceted diamond of style brilliant cut.

If the infrared beam strikes perpendicular to the table (Figure 2.10) the transmitted beam continues traveling in the same direction. In this case, the directions of both the incident beam and the transmitted beam lie along the normal to the culet of diamond contacted with polymer sample. Refractive index at interface between two materials – here, diamond and polymer – determines the angle for total internal reflection. Refractive index of diamond is 2.417 and that of polymer is 1.55. According to Snell's law, $\theta_c = \sin^{-1}(n_1/n_0)$, critical angle is 39.8°. The angle of incident at culet of diamond is 40.75°, which is greater than critical angle. As a result, infrared beam is totally reflected.

2.5.3 Infrared spectrum of a diamond.

The infrared spectrum of a diamond shows three different absorption regions: three- phonon (3900-2650 cm^{-1}), two-phonon (2650-1500 cm^{-1}), and one-phonon (1400-900 cm^{-1})). All these absorptions appear in the spectra of all diamonds [25].

Moreover, the weak absorption bands in the high wavenumber region are clearly observed. The left part of the spectrum shows some sharp peaks at 4496, 4168, 3236, 3107 and 2787 cm^{-1}which are caused by hydrogen impurities [26]. The right part of the spectrum shows more complicated bands and not only the intensity but also their position can change from sample to sample. The bands in this region have been associated with nitrogen defects [27]. The positions and intensities of these peaks depend on the sample analyzed. Figures 2.11-2.13 represent the infrared spectra corresponding to different types of defects that can be found in diamond structure [28].
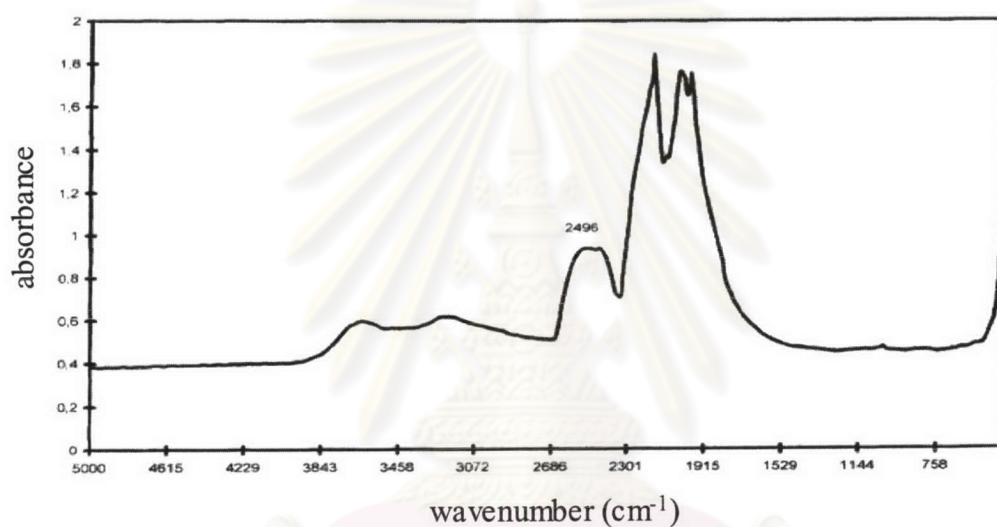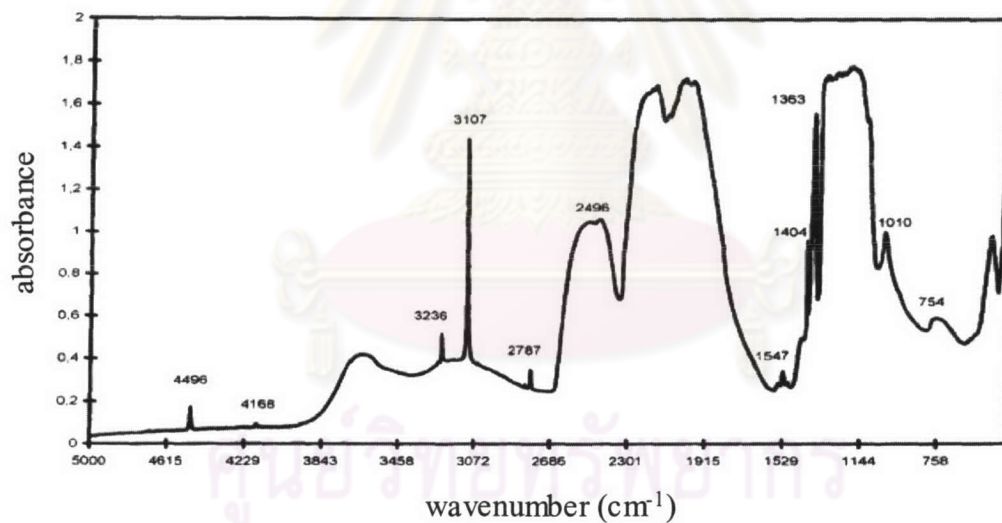

Figure 2.11 Spectrum of a brilliant cut diamond without impurities.
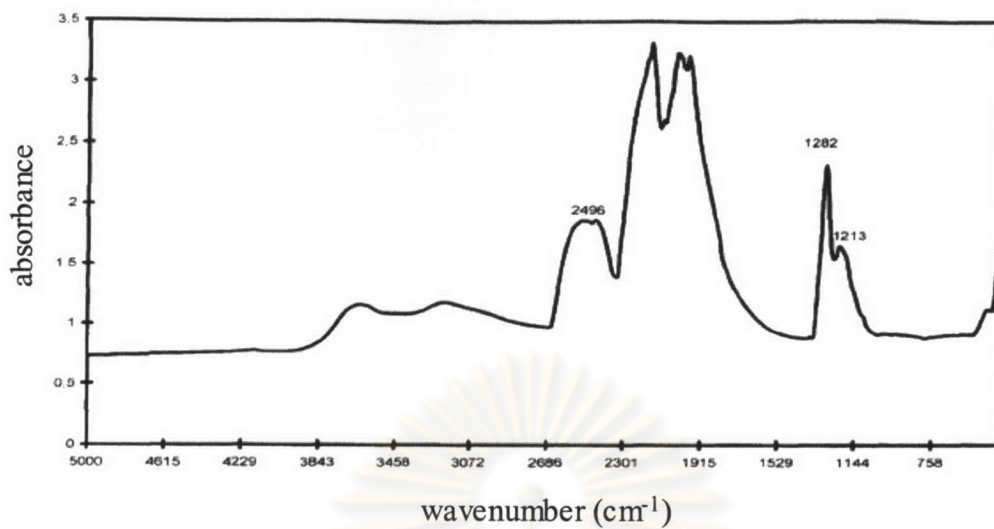
Figure 2.12 Spectrum of a brilliant cut diamond with nitrogen impurities of type IaA.

Figure 2.13 Spectrum of a brilliant cut with nitrogen impurities of type IaAB and also with hydrogen impurities.